

Experimental study of weak antilocalization effect in a high mobility InGaAs/InP quantum well

S.A. Studenikin^{*}, P.T. Coleridge, N. Ahmed[#], P. Poole and A. Sachrajda

Institute for Microstructural Sciences, National Research Council of Canada, Ottawa, Ontario, K1A 0R6, Canada

[#] Department of Physics, University Brunei Darussalam, Brunei Darussalam

(Dated: 25 February 2003)

The magnetoresistance associated with quantum interference corrections in a high mobility, gated InGaAs/InP quantum well structure is studied as a function of temperature, gate voltage, and angle of the tilted magnetic field. Particular attention is paid to the experimental extraction of phase-breaking and spin-orbit scattering times when weak anti-localization effects are prominent. Compared with metals and low mobility semiconductors the characteristic magnetic field $B_{tr} = \hbar/4eD$ in high mobility samples is very small and the experimental dependencies of the interference effects extend to fields several hundreds of times larger. Fitting experimental results under these conditions therefore requires theories valid for arbitrary magnetic field. It was found, however, that such a theory was unable to fit the experimental data without introducing an extra, empirical, scale factor of about 2. Measurements in tilted magnetic fields and as a function of temperature established that both the weak localization and the weak anti-localization effects have the same, orbital origin. Fits to the data confirmed that the width of the low field feature, whether a weak localization or a weak anti-localization peak, is determined by the phase-breaking time and also established that the universal (negative) magnetoresistance observed in the high field limit is associated with a temperature independent spin-orbit scattering time.

A . Introduction

With the growing interest in the spin properties of low-dimensional structures, particularly for spintronics and quantum information applications, there is a need for reliable experimental tools to obtain this information. For example, spin-orbit relaxation times can be determined by time-resolved optical methods^{1,2,3} but an alternative and complementary method is to use the weak antilocalization (WAL) effect. In metals, where it was thoroughly studied in the eighties^{4,5,6}, WAL is well understood, but for high mobility semiconductor structures some refinement is needed if it is to become a reliable tool for determining scattering parameters.

For diffusion dominated transport the characteristic magnetic field is $B_{tr} = \hbar/4eD$ where D is the diffusion constant and τ the scattering time. In metals B_{tr} is relatively large but in semiconductor samples it can be very small: e.g. in the high mobility 2-dimensional electron gas studied here, it is as small as 0.5 mT at zero gate voltage. Weak localization (WL) effects extend to fields several hundred times larger than this and even the very narrow WAL peak extends well beyond B_{tr} . It is not then valid to use low field approximations (which assume $B \ll B_{tr}$) to obtain experimental parameters⁷. In this paper we will address the issue of how to experimentally extract the phase-breaking (τ_ϕ) and spin-orbit (τ_{so}) time constants under these conditions. It will be experimentally established that both the WL and WAL effects have the same orbital origin. Further, it will be shown that even when there is a crossover from weak to strong spin-orbit coupling, marked by a change from negative (WL) to positive (WAL) magnetoresistance as $\tau_\phi = \tau_{so}$ increases, the characteristic width of the peak continues to be determined by τ_ϕ . To determine τ_{so} accurately requires that the whole curve, including the high field tail, be fitted.

B . Experimental

The sample studied was a high mobility, gated InGaAs quantum well structure grown by chemical beam epitaxy on an InP (100) substrate⁸. This sample was of a particular interest because it exhibited large spin-orbit effects. A cross-sectional layout view of the structure is shown in Fig.1. The quantum well is formed by 10 nm of $\text{In}_{0.53}\text{Ga}_{0.47}\text{As}$ ($x=0.53$) grown on an undoped InP buffer layer and separated from the Si-doped layer by a 30 nm spacer. A rectangular Hall-bar sample, width 0.2 mm and separation between adjacent potential probes 0.4 mm, was fabricated using optical lithography and wet etching. A gold gate was deposited on top of a 40 nm SiO_2 dielectric layer.

Experiments were performed in a He3 system (with temperatures to below 300 mK) in both perpendicular and tilted magnetic fields. Measuring currents were 100 nA or smaller. For precise

measurements in very small magnetic fields special attention must be paid to the accuracy of the magnetic field. A superconducting magnet was used with the persistent switch was removed to ensure all current delivered by the power supply passed through the magnet. The magnet power supply (Oxford Instruments IP S120-10) had a stability and reproducibility significantly better than 10^{-5} T. To overcome the problem of a trapped flux and the associated hysteresis in the magnet near zero field we established a protocol for the magnetic field history which was calibrated using a high sensitivity Hall probe. For most measurements the Hall voltage from the sample was measured simultaneously and used to confirm the accuracy of the magnetic field determined in this way.

Results of low-field Hall-effect measurements of the concentration and mobility as a function of gate voltage (V_g) are shown in Fig. 2. The concentration changes linearly with the gate voltage, as expected from a simple capacitor model, indicating there was no electric-field dependent charge accumulation between 2DEG and the gate. The straight line in Fig. 2 is calculated based on the parameters shown in Fig. 1 using an oxide thickness $d_{ox} = 40\text{nm}$ and dielectric constants $\epsilon_{ox} = 3.9$ and $\epsilon_{InP} = 12.6$. The electron mobility shown in Fig. 2 has a sub-linear gate voltage dependence, changing from 8 to $1\text{ m}^2/\text{Vs}$ as the gate voltage was reduced from 0 to -0.7 V. This corresponds to a characteristic magnetic field B_{tr} increasing from 0.5 mT at $V_g = 0\text{ V}$ to 140 mT at $V_g = -0.7\text{ V}$.

Fig. 3 shows an example of the magnetoresistance (MR) measured over a wide range of the magnetic field at several different temperatures. Four separate field regions can be distinguished. At high fields ($B > 0.3\text{ T}$) the Shubnikov-de Haas oscillations are visible; in an intermediate region there is a slow monotonic, temperature dependent, negative magnetoresistance. This parabolic term results from the electron-electron interaction effects^{4,9,10} and will not be discussed here. Focussing on the low field region ($B < 0.02\text{ T}$) both negative and positive MR components associated with quantum interference corrections are seen. It is commonly accepted that the negative MR is due to the WL effect and the central, very narrow, dip to the WAL effect. This dip, which appears only in samples where the spin-orbit scattering is strong, is so narrow that it could be used as an absolute zero-field sensor, with a precision of better than 10^{-5} T , in applications where it might be necessary to compensate the Earth's magnetic field.

The standard procedure to separate spin and orbital effects is to make measurements with magnetic field tilted away from the normal. Spin dependent terms, which depend on the total magnetic field, then become enhanced relative to orbital terms which depend only on the normal component of the field. Fig.4 shows MR traces for different tilt angles (θ) plotted as a function of the normal component $B \cos \theta$ ¹¹. If the WAL and WL components were to originate

from different mechanisms (e.g. WAL due to spin and WL due to orbital motion) a relative change in width of the two effects would be expected at different angles but in fact this is not so and the curves coincide. This implies that both the WL and WAL effects depend only on the normal component of magnetic field and that they both result from the orbital motion. It can be concluded that any independent spin degree of freedom has been suppressed by the spin-orbit coupling.

C. Weak anti-localization data in arbitrarily strong magnetic fields

The magnetoresistance due to interference corrections depends on three characteristic field values^{4,12}:

$$B_{tr} = \frac{h}{4eD}; B_{so} = \frac{h}{4eD_{so}} \quad \text{and} \quad B_{\phi} = \frac{h}{4eD_{\phi}}, \quad (1)$$

where $D = l^2/2\tau$ is the diffusion coefficient, l is the mean free path, and τ , τ_{so} and τ_{ϕ} are respectively the elastic scattering time, the spin-orbit relaxation time and the phase-breaking time.

To extract these parameters from the MR traces it is common to use the Hikami-Larkin-Nagaoka (HLN) equation⁷ but this is only valid for small magnetic fields, $B \ll B_{tr}$ when the magnetic length $l_B = \hbar/eB$ is larger than the mean free path. In the high mobility sample considered here B_{tr} is very small (only $4.6 \cdot 10^4$ T at $V_g = 0$) and B_{so} and B_{ϕ} are even smaller ($0.9 \cdot 10^4$ and $7 \cdot 10^6$ T respectively). As can be seen from Fig. 4 even the WAL peak extends beyond the small field limit and it is therefore incorrect to use the HLN equation to extract these parameters. The equation fails because it was derived in the diffusion limit with sums over multiple collisions replaced by integrals. For fields larger than B_{tr} , when most closed path trajectories involve only a small number of collisions (as few as three), the sums have to be explicitly evaluated. This situation was treated in ref. 13, in the absence of spin-orbit effects, with the prediction that there is a universal dependence $(B/B_{tr})^{-1} = \overline{p(B)}$ for the magnetoconductance at high fields. The more general case, when spin-orbit effects are included, was considered by Zduniak et al.¹². Their expressions, which include both WL and WAL corrections to the conductivity, in arbitrary magnetic fields are:

$$\overline{p(B)} = K (e^2/h) [F(x; s_1) + \frac{1}{2}F(x; s_2) - \frac{1}{2}F(x; \phi)] \quad (2)$$

with

$$\begin{aligned} F(x; i) &= x \sum_{n=0}^{\infty} \frac{P_n^3}{R_n^2} \\ P_n(x; i) &= \int_0^{(2-x)^{1/2}} dt \exp(-(1+i)t(2-x)^{1/2}) L_n(t^2) \\ L_n(t^2) &= \sum_{m=0}^n \frac{(-1)^m}{(n-m)!} \frac{n!}{m!} \left(\frac{t}{m}\right)^{2m} \end{aligned}$$

where L_n are Laguerre polynomials, $i = \phi, s_1$ or s_2 , and

$$x = \frac{B}{B_{tr}} = \frac{4eBD}{h}; \quad \phi = \frac{B_{\phi}}{B_{tr}}; \quad s_2 = \frac{B_{so}}{B_{tr}}; \quad s_1 = \phi + s_2; \quad s_2 = \phi + 2s_2;$$

Here (as is discussed below) an extra, empirical, coefficient K has been introduced as compared to ref. 12 to allow good fitting to the experimental data over the whole range of magnetic fields. To reduce computation time when fitting data the function $F(x; i)$ was calculated using 2000 Laguerre polynomials and stored numerically as a matrix of $F_{ij} = F(x_i; j)$ on a semi-logarithmic mesh. Values between defined points $(x_i; j)$ and $(x_{i+1}; j+1)$ were determined by linear interpolation.

Although the calculated quantity is that measured is σ_{xx} . Even in the absence of any interference corrections $\sigma_{xx} = \sigma_{xx} = (\sigma_{xx}^2 + \sigma_{xy}^2)$ has a small quadratic field dependence, which, in high mobility samples, cannot be ignored. It can be corrected for by comparing the calculated quantity $\sigma_{WL}(B)$ not with σ_{xx} but rather with $(1 - \sigma_{xx}) = 1 - \sigma_{xx} = 0$, which classically has no field dependence.

Figure 5 gives an example of experimental data of $(1 - \sigma_{xx})$ which compares with calculated values of σ_{WL} obtained from Eqn.(2) with $K = 1$. A reasonably good fit to the low field part of the experimental data can be obtained with $\phi = 0.005$ and $s_2 = 0.38$ but the calculated curve deviates significantly from the data at higher fields. In high-field region ($B/B_{tr} > 1$), where universal behaviour is expected^{12,13}. The high field tail can be fitted with a range of values of ϕ and s_2 provided only that they are small ($\phi, s_2 < 0.01$). Any adequate fit to the high field tail, however, leaves a large discrepancy in the low-field region ($B/B_{tr} < 1$). Conversely, although the shape of the

WAL peak depends mainly on τ , the turn-over from WAL to WL behaviour is determined essentially by τ_{so} . Values of τ and τ_{so} large enough to describe low field dependence properly are then too large to fit the high field part of the data. Exactly the same problem is also evident in other works, e.g. in Ref. 12 where universal behaviour of the magnetoresistance at high fields is reported and fitted using reasonable parameters but only at the expense of poor fits at low fields.

The problem of fitting the magnetoresistance associated with WAL effects in semiconductor structures, over a wide range of magnetic fields, is well known. Weak localization in semiconductors is more complex than in metals because of high electron mobilities and because new mechanisms involving spin orbit effects appear. One purpose of this paper is to alert theorists to this issue. As noted above, papers that consider WL effects in arbitrary magnetic fields, e.g. Ref. 12,13, are unable to adequately describe the experiments. Despite this it is possible to obtain estimates of the phase-breaking and spin-orbit scattering times from experimental MR curves that may have systematic errors but will nevertheless correctly reproduce gate voltage and temperature dependences. One commonly used procedure is to fit only the low field part of the MR using the HLN expression⁷. In this paper we use the more elaborate expression Eq.2 (with $K=1$) which coincides with HLN formula at small fields. Secondly, we fit data over the whole range of the magnetic field by introducing the extra, empirical coefficient K . Because we can provide no theoretical justification for the coefficient K , we present results for τ and τ_{so} determined with both $K=1$ and K allowed to vary.

The fits to the low field data with $K=1$ (see Fig.5) not only failed to describe the high field tail but also gave unreasonably large values for the spin-orbit parameter τ_{so} . For example the value of 0.38 used in Figure 5 corresponds to the unphysical value of approximately one for the parameter τ_{s2} in Eqn.(2). Examples of fits with K allowed to vary are shown in Fig.6. In this case fits for all temperatures gave $K=2.1 \pm 0.1$. For more negative gate voltages the high field data had essentially the same, universal, behaviour and could again be adequately fitted with $K=2$ although with an increased experimental uncertainty. To make the comparisons of τ and τ_{so} more meaningful it was therefore decided to fix K at 2 with a corresponding reduction in the uncertainty with which the other parameters could be determined.

With the empirically introduced coefficient K it was possible to achieve satisfactory fits to the data, over the whole field range, for all temperatures and gate voltages. We note that K does not appear to be a universal coefficient; in other samples¹⁴ values of K smaller than 2 were needed to fit the data. The failure of the theory with $K=1$ raises questions about other fitting procedures commonly used in the literature, in particular the HLN formula which, at low fields, is equivalent to Eqn.2 with $K=1$ ¹². Fitting to just the low field (WAL) region with $K=1$, i.e. relaxing the requirement that the high field behaviour be adequately described (see Fig. 5), gives values for the parameter τ several times smaller and τ_{so} several times larger than those obtained with $K=2$. Fitting to the low field region using the HLN equation gave very similar parameters but with even larger deviations at high fields.

While it is common to offset the theoretical curves to have a value of $\rho = 0$ at $B=0$ (as shown for example in Fig. 5) the theoretical values given by Eqn. 2 tend to zero in the limit of high magnetic field where both the WL and WAL effects are fully quenched. This means that fits made without any offset (for example those shown in Fig.6) determine the absolute values of the interference correction to the conductivity. The temperature dependence seen in Fig. 6 shows a universal behaviour at high fields increasing with the same slope but low field (WAL) behaviour has a strong temperature dependence. As a function of temperature τ is expected to change but τ_{so} remain constant^{4,5}. It is often assumed, when WAL is present, that the low field dependence is determined by τ_{so} and the high field with τ . This would imply a temperature dependent high field region but unchanged WAL peak, in direct contrast to what is observed experimentally. The calculated fits (solid lines in Fig. 6) did confirm this point.

The changing amplitude of the WAL peak corresponds to a temperature dependent phase-breaking time τ , and the "universal" high field slope corresponds to a value of τ_{so} that is essentially independent of the temperature. This happens when there is strong spin-orbit scattering, that is $\tau_{so} < \tau$.

We conclude therefore, perhaps counterintuitively, that the orbital motion (the phase-breaking time) determines the width of the central WAL peak, but the strength of the spin-orbit scattering (τ_{so}) controls the high field "universal" behaviour. This behaviour is reflected in the HLN formalism⁷ which although not strictly valid for the high mobility sample measured here reflects the correct physics and has the advantage it can be treated analytically. For small B ($B \ll B_c$) it gives

$$\rho = \frac{e^2}{h} \frac{1}{24} \left(\frac{B}{B_c} \right)^2 \left(\frac{\tau}{\tau_{so}} \right); \quad (3)$$

where

$$\left(\frac{\tau}{\tau_{so}} \right) = \frac{1}{(1 + \tau/\tau_{so})^2} + \frac{1}{(1 + 2\tau/\tau_{so})^2} - 1$$

The dimensionless function τ depends only on the ratio $\tau = \tau_{so}$. For $\tau_{so} \gg 1$, corresponding to pure WL, $\tau = 1$ and the standard expression, given for example in ref. 4, is recovered. In the opposite limit however, $\tau = \tau_{so} \ll 1$, the absolute value of τ is still equal to one but the sign changes. The characteristic width of the peak, in both limits, is therefore determined by τ , the amplitude by the ratio $\tau = \tau_{so}$. The change of sign for a ratio $\tau_{so} \approx 0.3$ not one, reflects the fact that the spin-orbit interaction is three dimensional in nature with three spin components to relax compared with one for the scalar phase breaking process.

The WAL peak is therefore so narrow because the width is determined not by τ_{so} but rather by τ , which can be extremely small in high mobility structures (e.g. 7×10^6 T here at $V_g = 0$). In the absence of spin-orbit scattering, there would be a WL peak, with the same extremely narrow width but of the opposite sign.

D. Discussion

In this section the temperature and gate voltage (concentration) dependence of the phase-breaking time and spin-orbit interaction constant will be discussed. In the absence of a theory that can satisfactorily describe the magnetoconductivity over the whole field range we present values of τ and τ_{so} determined using both $K=2$ and $K=1$ as it discussed earlier. Figure 8 shows the phase breaking time τ as a function of temperature extracted by fitting the data such as that shown in Fig. 7. For both $K=1$ and $K=2$ the behaviour is similar with a linear dependence at higher temperatures and an essentially reduced slope below 1 K. The solid line shows a theoretical limit due to the electron-electron scattering based on a Fermi-liquid model^{4,21}:

$$\frac{1}{\tau} = \frac{k_B T}{h} \frac{G_0}{G_0} \ln \frac{0}{2 G_0} \quad (4)$$

with $G_0 = e^2/h$, and where $k_B T \approx h$. It should be noted that in the literature an empirical coefficient of order 2 is often introduced to bring the experimental data into better agreement with Eq. 4^{10,19}. This model works well in metals, where Fermi energy is large and the electron gas can be considered as being very uniform^{4,5}, but a saturation of τ is usually reported at low temperatures (see e.g. ref. 5). Similar behavior is observed in Fig. 7: at high temperatures τ determined using $K=2$ increases linearly with decreasing temperature with the expected slope and there is a saturation below 1 K. For $K=1$ the behaviour is qualitatively similar although less pronounced. In both cases the values at high temperatures is a factor of two or three smaller than expected in Fermi-liquid model. The saturation below 1 K suggests some additional phase-breaking mechanisms limit τ . Possibilities include inhomogeneous distribution of alloy composition, interface roughness or doping concentration variations^{18,20,22}. In high mobility samples such as that studied here small fluctuating magnetic fields may also be playing a role. The maximum value of $\tau \approx 100$ ps corresponds to $B \approx 0.012$ mT. This is an extremely small field, several times smaller than the Earth's magnetic field, so any fluctuating or micro-scale effective magnetic field of this magnitude would affect the very narrow WAL peak and appear as a phase-breaking mechanism. Permanent dc magnetic fields, such as the Earth's field, would lead only to an arbitrary shift in the position of the peak and in-plane components of the field would also have no effect. (cf Fig. 4.)

While any detailed analysis of the mechanisms of phase breaking is beyond the framework of this paper but it can be concluded that the WAL effect provides a useful tool for determining and controlling the phase breaking time. In the sample used here the value of about 100 ps corresponds to a phase breaking length $l = 20 - 40$ nm.

Gate voltage dependence of the magnetoconductivity is shown in Fig. 8. In this figure all the curves shifted vertically to coincide at $B = 0$. Rather surprisingly, when plotted in this way, universal behaviour is observed at low magnetic fields ($B < B_{tr}$) with the WAL peak for different gate voltage data collapsing onto a single logarithmic curve. Indeed, the low field WAL peak in Fig. 8 now shows a similar kind of $\ln(B)$ dependence seen in the high-field (WL) part but with the opposite sign.

The results from fitting this data are plotted in Fig. 9 as a function of the conductivity to be able to compare the results with Fermi-liquid model (Eq. 4). A gain two values of K have been used and in both cases the variation of τ is much slower than is predicted theoretically by the Fermi-liquid model Eq. (4). While it is not clear which of the curves is correct they both lie below the theoretical one and have a slower dependence on conductivity. This may be associated with the fact that the measurements were made at the lowest temperature and therefore just be reflecting the saturation observed in the temperature dependence (Fig. 7).

As noted above the width of the WAL feature depends on τ , but the amplitude and the transition to the high field tail also depends on τ_{so} . The physics describing the damping of the spin-orbit interaction is more complicated than for the dephasing. To describe the WAL effect a spin-dependent vector potential is required with a three dimensional character^{23,24,25}. Different spin-orbit relaxation mechanisms are not additive and more complicated expressions, with more fitting parameters, should be used to describe experiments. If, however, only one spin-orbit mechanism

dominates, as seems to be the case here, a single scalar parameter τ_{so} should suffice which can then be treated on the same footing as τ . The values of τ_{so} determined from fits to the field dependences as a function of density (Fig. 8), are plotted in Fig. 10 (a), again for $K=1$ and $K=2$. The spin-orbit relaxation time is significantly smaller than τ (and only a few times larger than transport relaxation time). For $K=2$ τ_{so} increases from 12 to 19 ps as the concentration decreases from 3.5 to $1.5 \times 10^{11} \text{ cm}^{-2}$; for $K=1$ case the deduced values of τ_{so} are even smaller. Small values of τ_{so} are consistent with the strong spin-orbit coupling in the InGaAs which means that any elastic scattering event has a high probability of also involving spin scattering.

Two major spin-orbit scattering mechanisms are expected for 2DEG systems such as that considered here: the Dresselhaus term, associated with the bulk zinc-blend crystal inversion asymmetry and the Rashba term, associated with a built-in electric field.²⁶ To distinguish which mechanism dominates it is helpful to consider the dependence of $B_{so} = \hbar/(4eD_{so})$ on electron concentration^{26,27,28}. In particular the Dresselhaus term is expected to increase with increasing carrier density. For example, in a GaAs/AlGaAs heterostructure a quadratic increase of B_{so} with density is predicted and was observed experimentally²⁷. Fig. 10 (b) shows B_{so} as a function of electron concentration. (Note that though B_{so} is inversely proportional τ_{so} the stronger density dependence of D means B_{so} also decreases with density). The approximately inverse parabolic dependence that is observed cannot be attributed to the Dresselhaus mechanism.

The Rashba term, which appears in asymmetric quantum wells, contributes a term $H_R = [\frac{\hbar}{4m} k]_z$ to the Hamiltonian with the coefficient proportional the expectation value of the electric field in the well. In the literature the role of interfaces in the Rashba mechanism is somewhat controversial. Within the effective mass approximation the expectation value of a (smooth) potential gradient integrated over the whole space is always zero^{24,29}. More generally, the interfaces should be treated separately and with contributions that may be as large (or even larger) as that from the quantum well²⁹. The two interfaces in a quantum well usually have different properties, because of differences in the growth process. Changing the gate voltage will therefore not only change the average built-in electric field in the well but also the relative interaction of the electrons with the different interfaces.

The density dependence seen in Fig. 10 (b) is of the opposite sign to that expected for a simple triangular conning potential. Simulations have shown, however, that this kind of functional dependence might be explained qualitatively by the built-in electric field²⁸ (excluding the effect of the interfaces) provided the background doping of the buffer layer (which contributes $2.2 \times 10^{11} \text{ cm}^{-2}$ carriers to the quantum well) is also taken into account. However, the magnitude of the effect is larger than expected and a more detailed study, outside the scope of the present paper, is needed to settle this point.

E. Conclusions

Interference corrections to the conductivity have been studied in a high-mobility InGaAs/InP quantum well with the particular intent of examining the WAL effect and refining the procedures needed to establish it as a tool for gaining information about phase-breaking and spin-orbit coupling processes. When the magnetoresistance was examined over a wide range of magnetic fields $0 < B = B_{cr} < 100$ it was found that functional dependence given in ref. 12 could not adequately describe the data. Reasonable fits could be obtained by introducing an empirical amplitude factor $\gamma \approx 2$. The reason for this disagreement is not understood and it would obviously be interesting to make similar measurements and analysis, over a wide field range, in other semiconductor systems. One possible reason is that the spin-orbit coupling is sufficiently strong in this particular InGaAs QW sample that the theory¹² is starting to fail because the condition $\tau_{so} \gg \tau$ is not well satisfied. In this case an alternative approach, based perhaps on a spin-dependent vector potential²³ needs to be developed.

Despite this disagreement several conclusions can be drawn from this study, summarized as follows. The WAL and WL effects both have an orbital origin and depend only on the perpendicular component of the magnetic field. For $\gamma = \tau_{so} = 1$ the central, low field peak, has WL character and for $\gamma = \tau_{so} = 1$ WAL character, but in both cases the width of the low-field peak is determined only by τ . The high field dependence is universal with the cross-over from the low field behaviour determined by the ratio $\gamma = \tau_{so}$.

The spin-orbit scattering time is small, between about 12 and 18 ps, and only weakly dependent on the electron concentration. As has been found in many other studies the experimentally determined dependence of τ on temperature and gate voltage cannot be satisfactorily described by Fermi-liquid theory, some additional phase-breaking mechanisms appear to be present.

Overall, we have demonstrated it is possible to use gate voltage to control the strength of the spin-orbit interaction. It was also shown that the magnetoresistance associated with the quantum interference corrections provides a powerful tool for controlling and studying the interplay between the phase-breaking time and spin-orbit coupling in low-dimensional structures. However, a theoretical understanding of these effects is still not complete, particularly for arbitrary magnetic field strengths and strong spin-orbit coupling.

F . Acknowledgements

We would like to acknowledge fruitful discussions with: Yu. Lyanda-Geller, Geof Aers, Boris Narozhny, Chandre Dharmawardana and Sergei Dickmann.

-
- ¹ S.A.Wolf, D.D.Awschalom, R.A.Buhrman, J.M.Daughton, S.von-Molnar, M.L.Roukes, A.Y.Chitchekanova, and D.M.Tregger, *Science* 294, 1488 (2001)
 - ² D.D.Awschalom, *Physica E* 10, 1 (2001)
 - ³ G.Salis, Y.Kato, K.Ensslin, D.C.Driscoll, A.C.Gossard, and D.D.Awschalom, *Nature* 414, 619 (2001)
 - ⁴ B.L.Altshuler, and A.G.Aronov, in *Electron-Electron Interactions in Disordered Systems*, edited by A.L.Efros and M.Pollak, North Holland, Amsterdam, 1985, p.1
 - ⁵ G.Bergman, *Physics Reports* 107, 1 (1984)
 - ⁶ S.Chakravarty and A.Schmid, *Physics Reports* 140,193 (1986)
 - ⁷ S.Hikami, A.Larkin and Y.Nagaoka, *Prog.Theor.Phys.* 63,707 (1980)
 - ⁸ J.Lefebvre, P.J.Poole, J.Fraser, G.C.Aers, D.Chithrani, and R.L.Williams *J.Cryst.Growth* 234, 391 (2002)
 - ⁹ A.Houghton, J.R.Senna and S.C.Ying, *Phys.Rev.B* 25, 2196 (1982)
 - ¹⁰ G.M.Minkov, O.E.Rut, A.V.Germenenko, A.A.Sherstobitov, V.I.Shashkin, O.I.Khrykin, and V.M.Daniltsev, *Phys.Rev.B* 64, 235327 (2001)
 - ¹¹ It should be noted this data was taken at the lowest temperatures and using a measuring current of only 30 nA to avoid possible heating problems. The noise is therefore larger than for other data.
 - ¹² A.Zduniak, M.I.Dyakonov, and W.Knap, *Phys.Rev.B* 56, 1996 (1997)
 - ¹³ V.M.Gasparyan, and A.Yu.Zyuzin, *Sov.Phys.Solid State* 27, 999 (1985)
 - ¹⁴ S.A.Studenikin, P.T.Coleridge (unpublished)
 - ¹⁵ H.Fukuyama, in *Electron-Electron Interactions in Disordered Systems*, edited by A.L.Efros and M.Pollak, North Holland, Amsterdam, 1985, p.155
 - ¹⁶ P.A.Lee and T.V.Ramakrishnan, *Reviews of Modern Physics* 57, 287 (1985)
 - ¹⁷ G.M.Minkov, A.V.Germenenko, V.A.Larionova, S.A.Negashev and I.V.Gomyi, *Phys.Rev.B* 61, 13164 (2000)
 - ¹⁸ G.M.Minkov, A.V.Germenenko, O.E.Rut, A.A.Sherstobitov, B.N.Zvonkov, E.A.Uskova, and A.A.Birukov, *Phys.Rev.B* 64 (2001)
 - ¹⁹ A.M.Kreshchuk, S.V.Novikov, T.A.Polyanskaya, and I.G.Savel'ev, *Sov.Phys.Semicond.* 61, 391 (1997); T.A.Polyanskaya, and Yu.V.Shmatsev, *Sov.Phys.Semicond.* 23, 1 (1989)
 - ²⁰ A.V.Germenenko, G.M.Minkov, and O.E.Rut, *Phys.Rev.B* 64, 165404 (2001)
 - ²¹ B.L.Altshuler, A.G.Aronov and D.E.Khmelnitskii, *L.Phys.C* 15, 7367 (1982)
 - ²² H.Mathur, and H.U.Baranger, *Phys.Rev.B* 64, 235325 (2001)
 - ²³ Yu.Lyanda-Geller, *Phys.Lett.* 80, 4273 (1998)
 - ²⁴ F.G.Pikus, and G.E.Pikus, *Phys.Rev.B* 51, 16928 (1995)
 - ²⁵ S.V.Iordanskii, Yu.B.Lyanda-Geller, and G.E.Pikus, *JETP Lett.* 60, 206 (1994)
 - ²⁶ W.Knap, C.Skierbiszewski, A.Zduniak, E.Litwin-Staszewska, D.Bertho, F.Kobbi, J.L.Robert, G.E.Pikus, F.G.Pikus, S.V.Iordanskii, V.Mosser, K.Zekentes, and Yu.B.Lyanda-Geller, *Phys.Rev.B* 53, 3912 (1996)
 - ²⁷ P.D.Dresselhaus, C.M.A.Papavassiliou, R.G.Wheeler, and R.N.Sacks, *Phys.Rev.Lett.* 68, 106 (1992)
 - ²⁸ G.L.Chen, J.Han, T.T.Huang, S.Datta, and D.B.Janes, *Phys.Rev.B* 47, 4084 (1993)
 - ²⁹ L.G.Gerchikov, and A.V.Subashiev, *Semiconductors*, 26, 73 (1992)

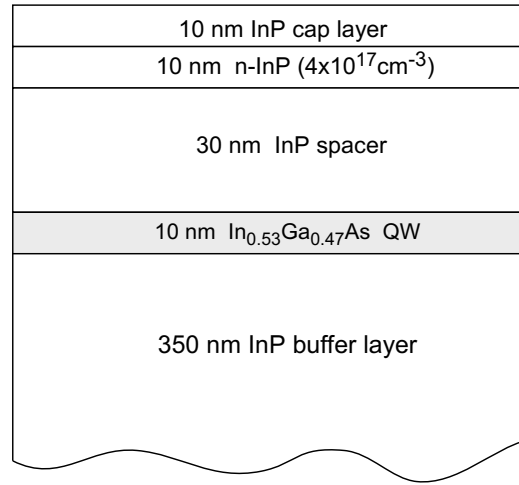


FIG . 1: Cross-sectional layout view of the InGaAs/InP quantum well structure.

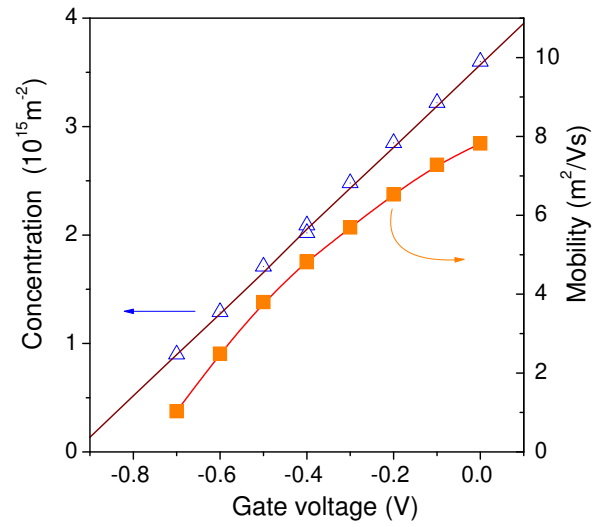


FIG . 2: Results of Hall-effect measurements of the electron concentration and mobility vs gate voltage.

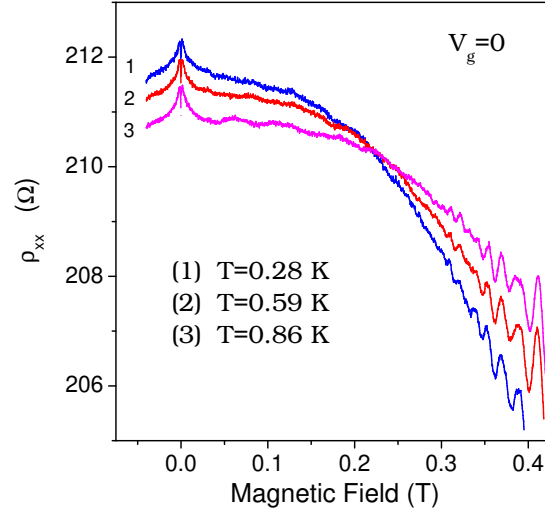


FIG. 3: Magnetoresistance traces from the InGaAs/InP quantum well structure at different temperatures for a wide range of the magnetic fields.

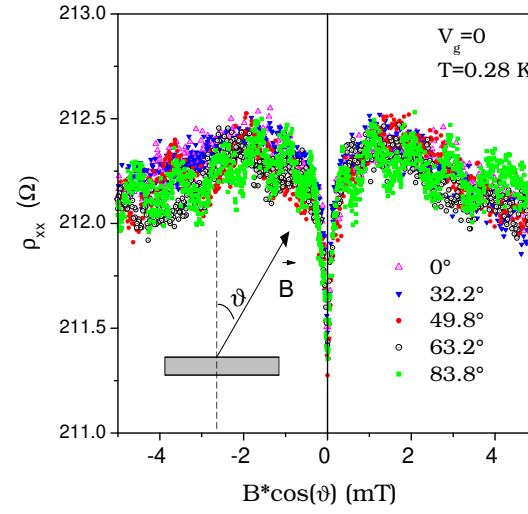


FIG. 4: Low field magnetoresistance attributed to quantum interference corrections in tilted magnetic fields plotted as a function of the normal component of magnetic field.

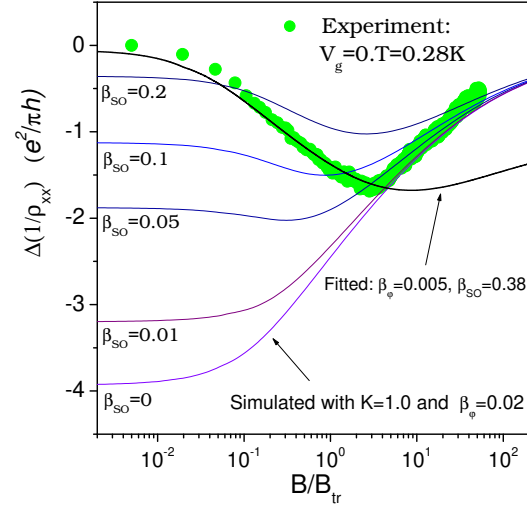


FIG . 5: Conductivity plotted against normalized magnetic field. Points are experimental data at $V_g = 0$ and $T = 0.28$ K. Lines are simulated dependencies from eq.(2), all with $K = 1$.

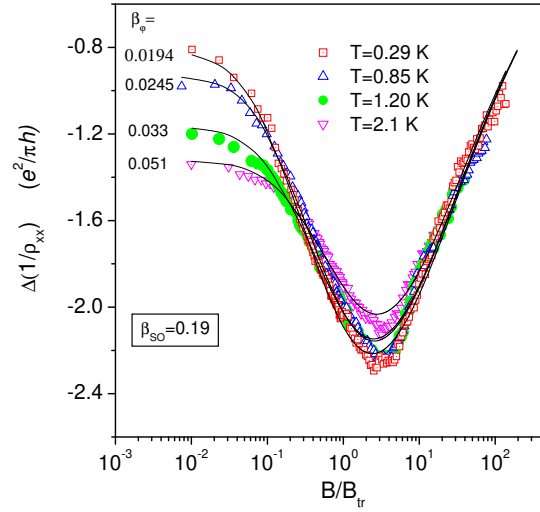


FIG . 6: Magnetoconductivity, at different temperatures and with $V_g = 0$, plotted against normalized magnetic field. Lines are fitted dependencies with Eq.(2) using $K = 2$. The experimental data are offset to coincide with the theoretical curves which approach zero in strong magnetic fields. A universal behavior is observed in high magnetic field region. Amplitude of the WAL peak at $B = 0$ strongly depends on temperature.

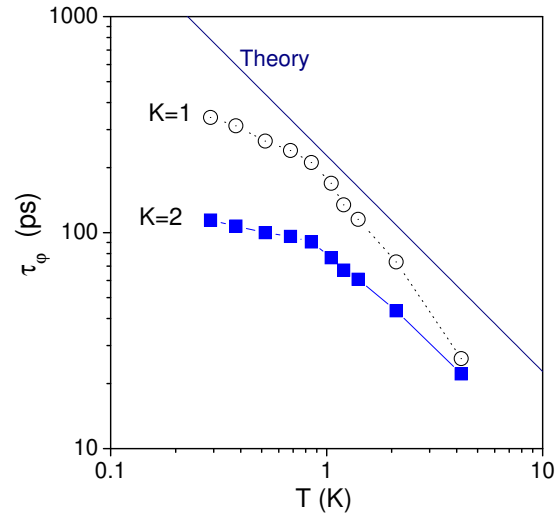


FIG. 7: Phase-breaking time τ_ϕ , as a function of temperature, extracted by fitting data in Fig. 6 with $K=2$ (solid squares) and $K=1$ (open circles). Solid line is a theoretical limit due to the electron-electron scattering (eq. 4).

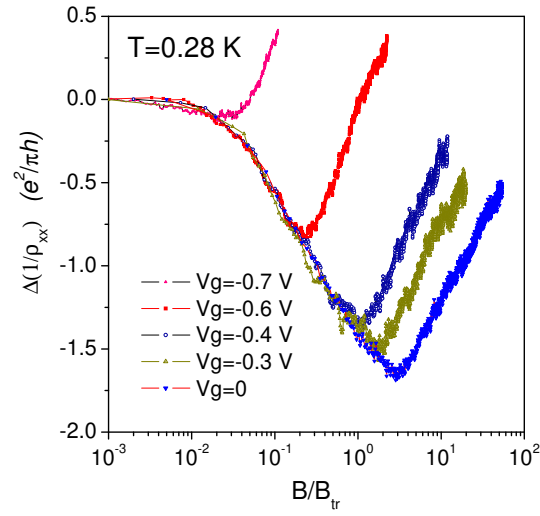


FIG. 8: Magnetoconductivity plotted against normalized magnetic field for different gate voltages. The experimental curves are offset to have the same value at $B=0$.

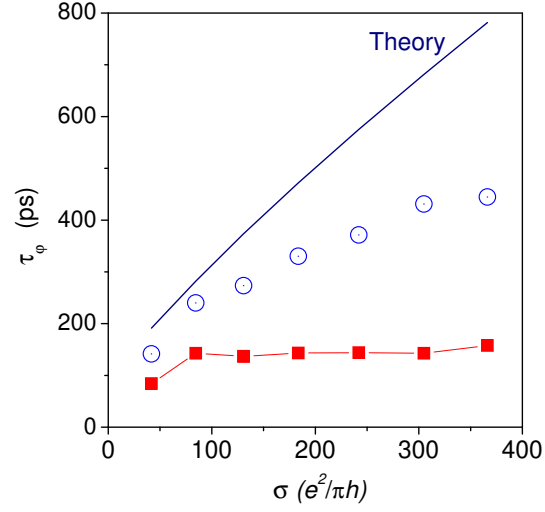


FIG. 9: Phase braking time vs conductivity. Line is theoretical prediction based on Fermi liquid model eq. 4, points are experimental results obtained by fitting data in Fig. 8 with eq. 2 using $K = 1$ (open circles) and $K = 2$ (solid squares).

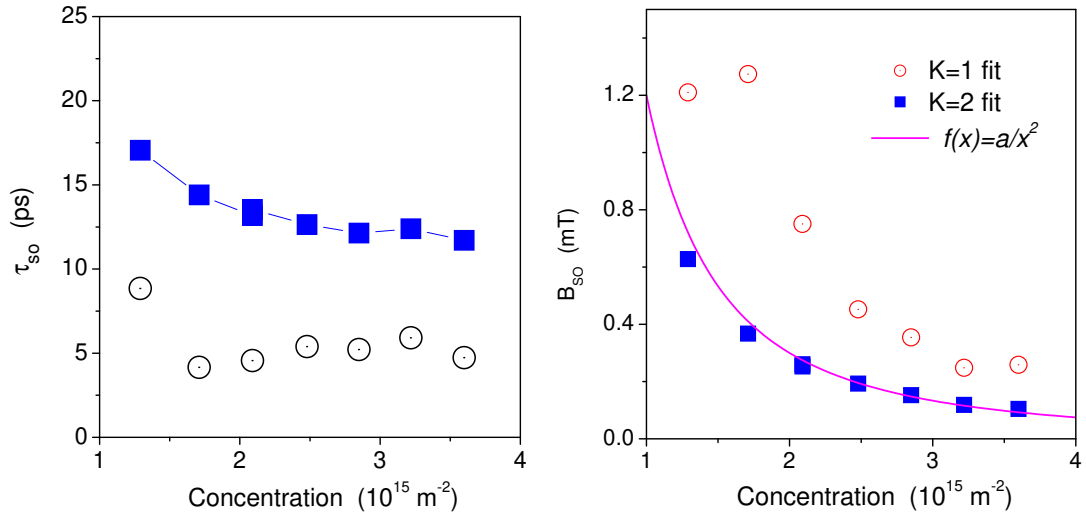


FIG. 10: (a) Spin-orbit scattering time as a function of the 2DEG concentration determined from fits to the data in Fig. 8 using $K = 1$ (open circles) and $K = 2$ (solid squares). (b) Characteristic magnetic field value B_{so} as a function of the electron concentration calculated on the basis of the data in Fig. 10 (a) and Fig. 2. Solid line is a fit proportional to inverse square of the electron concentration.